Nonequilibrium phase transition in an exactly solvable driven Ising model with friction

Alfred Hucht
Fakultät für Physik und CeNIDE, Universität Duisburg–Essen, D-47048 Duisburg, Germany
(Received 3 September 2009; published 30 December 2009)

A driven Ising model with friction due to magnetic correlations was proposed by Kadau *et al.* [Phys. Rev. Lett. **101**, 137205 (2008)]. The nonequilibrium phase transition present in this system is investigated in detail using analytical methods as well as Monte Carlo simulations. In the limit of high driving velocities v the model shows mean-field behavior due to dimensional reduction and can be solved exactly for various geometries. The simulations are performed with three different single spin-flip rates: the common Metropolis and Glauber rates as well as a *multiplicative* rate. Due to the nonequilibrium nature of the model all rates lead to different critical temperatures at $v>0$, while the exact solution matches the multiplicative rate. Finally, the crossover from Ising to mean-field behavior as function of velocity and system size is analyzed in one and two dimensions.

DOI: 10.1103/PhysRevE.80.061138 PACS number(s): 05.50.+q, 68.35.Rh, 04.20.Jb

I. INTRODUCTION

Magnetic contributions to friction due to spin correlations have attracted increasing interest in recent years. One interesting aspect is the energy dissipation due to spin waves in magnetic force microscopy, where magnetic structures are investigated by moving a magnetic tip over a surface [1–3]. On the other hand, magnetic friction is also present in bulk magnetic systems which are in close proximity. In this context, Kadau *et al.* [4] proposed a simple model for magnetic friction mediated solely by spin degrees of freedom. In this model an Ising spin system is moved over a second spin system with constant velocity v along a boundary. This permanent perturbation drives the system to a steady state far away from equilibrium, leading to a permanent energy flow from the boundary to the heat bath.

This problem can be analyzed for several different geometries in one, two, and three dimensions, as shown in Fig. 1: besides the original problem of two half-infinite two-dimensional systems moving along the one-dimensional boundary, denoted by $2d_b$ in the following, we will consider the homogeneous cases 1d and 2d where all spins are at the boundary, as well as the experimentally relevant three-dimensional case ($3d_b$). Additionally, we will extend the analysis to sheared systems in two [5–7] and three [8] dimensions, denoted by 1+1d and 2+1d. These systems are experimentally accessible within the framework of shear flow in binary liquid mixtures (for a review, see [9]), though with conserved order parameter, while we deal with a non-conserved order parameter.

This model has some similarities to the *driven lattice gas* (DLG) proposed by Katz *et al.* [10] (see [11] for a review), where a system is driven out of equilibrium by an applied field which favors the motion of particles in one direction. We will discuss these similarities throughout this work.

The paper is organized as follows: in the first part we will introduce the model and geometries and present, in the second part, an exact solution of the model in the limit of high driving velocities $v\to\infty$, which will be checked numerically in the last part using Monte Carlo (MC) simulations. There we will also investigate the case of finite velocities v.

II. MODEL

Let us start with the simplest case denoted 1d in Fig. 1 and consider two Ising chains with spin variables $\sigma=\pm 1$, nearest-neighbor coupling $K=\beta J$ ($\beta=1/k_B T$ and we set $k_B=1$) and $L_\parallel$ sites each, interacting with boundary coupling $K_b=\beta J_b$ and moving along each other with relative velocity v. In the Monte Carlo simulation the upper system is moved v times by one lattice constant a_0 with respect to the lower system during each random sequential Monte Carlo sweep (MCS). As one MCS corresponds to a typical spin-relaxation time $t_0=O(10^{-8}\ \mathrm{s})$ [12] and $a_0=O(10^{-10}\ \mathrm{m})$, the velocity v is given in natural units $a_0/t_0=O(1\ \mathrm{cm/s})$ (we will set $a_0=t_0=1$ in the following).

To simplify the implementation, instead of moving the upper part of the lattice with respect to the lower part we reorder the couplings at the boundary with time. This procedure is analogous to the Lees-Edwards or *moving boundary condition* in molecular-dynamics simulations of fluids [13] and leads to a system as shown in Fig. 2. Assuming periodic boundary conditions (PBCs) $\sigma_{k,l}\equiv\sigma_{k,l \bmod L_\parallel}$ in the parallel direction, the time-dependent Hamiltonian reads

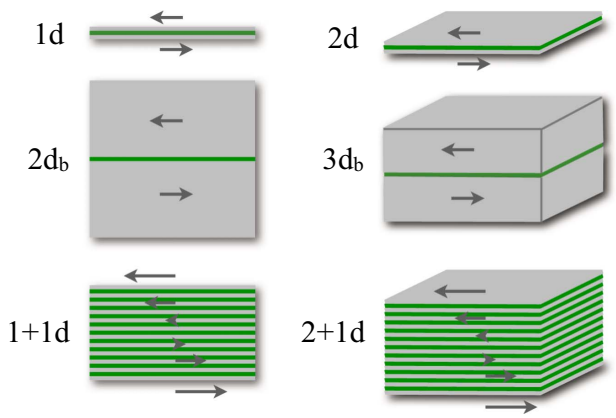

FIG. 1. (Color online) Overview of the geometries considered in this work. The gray regions are the magnetic systems, while the green (dark) regions are the moving boundaries. The arrows indicate the motion of the subsystems.

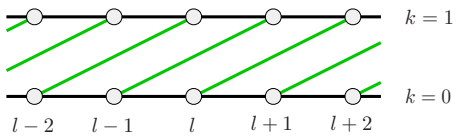

FIG. 2. (Color online) Sketch of geometry 1d after $\Delta=2$ moves. Spin $\sigma_{0,l}$ interacts with spin $\sigma_{1,l+2}$ with coupling J_b [green (gray) lines], while all other couplings are J (black lines).

$$\beta\mathcal{H}(t) = -K\sum_{k=0}^{1}\sum_{l=1}^{L_\parallel}\sigma_{k,l}\sigma_{k,l+1} - K_\mathrm{b}\sum_{l=1}^{L_\parallel}\sigma_{0,l}\sigma_{1,l+\Delta(t)}, \quad (1)$$

with the time-dependent displacement

$$\Delta(t) = vt. \quad (2)$$

The second geometry considered in this work is the $2\mathrm{d}_\mathrm{b}$ case shown in Fig. 3, which already was investigated by Kadau *et al.* [4]. Here we have a square lattice with $L_\parallel \times L_\perp$ sites and periodic boundary conditions in both directions, i.e., $\sigma_{k,l} \equiv \sigma_{k \bmod L_\perp, l \bmod L_\parallel}$. Note that especially $\sigma_{L_\perp,l} \equiv \sigma_{0,l}$. The Hamiltonian of this system becomes

$$\beta\mathcal{H}(t) = -\sum_{k=1}^{L_\perp}\sum_{l=1}^{L_\parallel} K\sigma_{k,l}\sigma_{k,l+1} + K_{\perp,k}\sigma_{k,l}\sigma_{k+1,l+\Delta_k(t)}, \quad (3)$$

with $\Delta_k(t) \equiv 0$ and $K_{\perp,k}=K$ for all rows except row $k=0$, where the couplings to row $k=1$ are shifted with constant velocity $\Delta_0(t) \equiv \Delta(t)=vt$. The coupling $K_{\perp,0} \equiv K_\mathrm{b}$ across the boundary is allowed to be different from K. For $v=0$ and $J_\mathrm{b}=J=1$ this system simplifies to the two–dimensional (2D) Ising model in equilibrium, which was solved exactly by [14] and shows a continuous phase transition at

$$T_{\mathrm{c,eq}} = \frac{2}{\ln(1+\sqrt{2})} = 2.269\ 185\ 3\ldots. \quad (4)$$

Note that both systems are translationally invariant in $\parallel$ direction under the transformation $l \to l+1$ and obey reflection symmetry at the boundary under $k \to 1-k$.

III. EXACT SOLUTION AT HIGH VELOCITIES

In Ref. [4] it was shown that for high velocities $v \gg 1$ the properties of the $2\mathrm{d}_\mathrm{b}$ system become independent of v. This

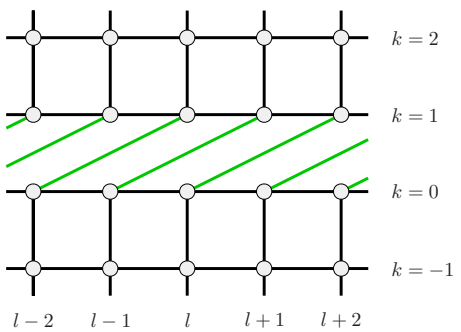

FIG. 3. (Color online) Sketch of geometry $2\mathrm{d}_\mathrm{b}$ after $\Delta=2$ moves.

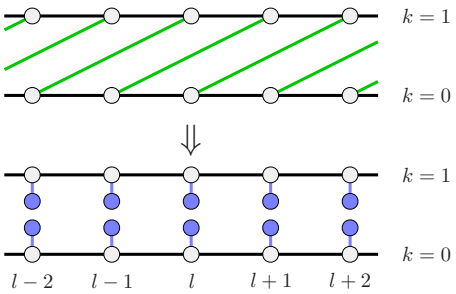

FIG. 4. (Color online) Mapping of the 1d driven system, shown for $\Delta=2$, on two disconnected 1D systems with fluctuating fields.

can be understood as follows: in the limit $v \to \infty$ the interaction $K_\mathrm{b}\sigma_{0,l}\sigma_{1,l+\Delta(t)}$ across the driven boundary becomes uncorrelated, as, in the Monte Carlo simulations, at large v the spin $\sigma_{1,l+\Delta(t)}$ is different in every trial step and can, for simplicity, be a randomly chosen spin $\sigma_{1,\mathrm{rnd}}$ from row 1. Note that this simplification was checked within the simulations and indeed gave the same results, enabling us to perform simulations *at* $v=\infty$. Thus the boundary coupling can be replaced by the action of a fluctuating boundary field μ, e.g.,

$$\sigma_{0,l}\sigma_{1,l+\Delta(t)} \to \sigma_{0,l}\sigma_{1,\mathrm{rnd}} \to \sigma_{0,l}\mu_{0,l}, \quad (5)$$

with stochastic variables $\mu_{kl}=\pm 1 (k=0,1)$ under the constraint $\langle\mu_{kl}\rangle=\langle\sigma_{kl}\rangle=m_\mathrm{b}$, where m_b denotes the magnetization at the driven boundary. Here we used the translation symmetry $\langle\sigma_{kl}\rangle=m_k$ and the reflection symmetry at the boundary, $m_k=m_{1-k}$. In Fig. 4 this mapping of the driven system onto a system with fluctuating boundary fields is illustrated for the 1d case. The next step will be to map the fluctuating fields onto static fields by integrating out the degrees of freedom μ_{kl}.

A. Ising model in a fluctuating field

Consider a general Ising model with arbitrary couplings K_{ij} in a static external field h_i^{ext} and additional fluctuating fields of strength k_i (note the factor β in all field quantities)

$$\beta\mathcal{H}_\mu = -\sum_{i<j} K_{ij}\sigma_i\sigma_j - \sum_i (h_i^{\mathrm{ext}} + k_i\mu_i)\sigma_i, \quad (6)$$

where the $\mu_i=\pm 1$ are stochastic variables at site i with given average

$$\langle\mu_i\rangle = m_i. \quad (7)$$

As this condition is given *a priori*, averages containing μ_i can be calculated using the trace formula

$$\mathrm{Tr}_\mu f(\mu_i) = \sum_{\mu_i=\pm 1} f(\mu_i)p_i(\mu_i) \quad (8)$$

with the probability distribution $p_i(\mu_i)=(1+\mu_i m_i)/2$, as then

$$\langle\mu_i\rangle = \mathrm{Tr}_\mu\, \mu_i = \sum_{\mu_i=\pm 1} \mu_i p_i(\mu_i) = m_i$$

as assumed. With the decomposition

$$\beta\mathcal{H}_\mu = \beta\mathcal{H}_0 - \sum_i k_i\mu_i\sigma_i, \tag{9}$$

the degrees of freedom μ in the partition function $\mathcal{Z}$ can be traced out,

$$\begin{aligned}\mathcal{Z} &= \mathrm{Tr}_{\sigma\mu}\, e^{-\beta\mathcal{H}_\mu} = \mathrm{Tr}_\sigma\, e^{-\beta\mathcal{H}_0}\, \mathrm{Tr}_\mu \prod_i e^{k_i\mu_i\sigma_i} \\ &= \mathrm{Tr}_\sigma\, e^{-\beta\mathcal{H}_0} \prod_i \sum_{\mu_i=\pm 1} e^{k_i\mu_i\sigma_i} p_i(\mu_i) \\ &= \prod_i \cosh k_i\, \mathrm{Tr}_\sigma\, e^{-\beta\mathcal{H}_0} \prod_i [1 + \sigma_i m_i \tanh k_i], \end{aligned} \tag{10}$$

where we used the fact that $\sigma_i = \pm 1$.

On the other hand, the Hamiltonian of the equilibrium Ising model without fluctuating fields in a static field h_i can be written as

$$\beta\mathcal{H}_{\mathrm{eq}} = -\sum_{i<j} K_{ij}\sigma_i\sigma_j - \sum_i h_i\sigma_i = \beta\mathcal{H}_0 - \sum_i b_i\sigma_i, \tag{11}$$

with $\mathcal{H}_0$ from Eq. (9) if we let $b_i = h_i - h_i^{\mathrm{ext}}$. The partition function of this model clearly fulfills

$$\begin{aligned}\mathcal{Z}_{\mathrm{eq}} &= \mathrm{Tr}_\sigma\, e^{-\beta\mathcal{H}_{\mathrm{eq}}} \\ &= \mathrm{Tr}_\sigma\, e^{-\beta\mathcal{H}_0} \prod_i e^{b_i\sigma_i} \\ &= \prod_i \cosh b_i\, \mathrm{Tr}_\sigma\, e^{-\beta\mathcal{H}_0} \prod_i [1 + \sigma_i \tanh b_i]. \end{aligned} \tag{12}$$

Comparing Eqs. (10) and (12), we conclude that under the condition

$$\tanh b_i = m_i \tanh k_i, \tag{13}$$

the partition function $\mathcal{Z}$ can be expressed in terms of $\mathcal{Z}_{\mathrm{eq}}$,

$$\mathcal{Z} = \left. \prod_i \frac{\cosh k_i}{\cosh b_i} \mathcal{Z}_{\mathrm{eq}} \right|_{\mathrm{Eq.(13)}}. \tag{14}$$

To summarize, the coupling with strength k_i to fluctuating fields $\mu_i = \pm 1$ with given average $\langle\mu_i\rangle = m_i$ can be written as coupling to static effective fields b_i with strength given by Eq. (13). In the next section we will use this mapping to exactly solve the driven Ising model for high velocities $v \to \infty$.

B. Application to the driven Ising model

The general condition [Eq. (13)] for the effective static fields b_i simplifies for the systems considered in this work: as all boundary spins are equivalent, $m_i = m_{\mathrm{b}}$, with coupling $k_i = K_{\mathrm{b}}$, leading to a uniform effective field $h_{\mathrm{b}} = \mathrm{artanh}(m_{\mathrm{b}} \tanh K_{\mathrm{b}})$ at the boundary, as we assume no additional external fields, $h_i^{\mathrm{ext}} = 0$. Inserting this into the equilibrium expression for the boundary magnetization $m_{\mathrm{b,eq}}(K, h_{\mathrm{b}}) = \partial \ln \mathcal{Z}_{\mathrm{eq}} / \partial h_{\mathrm{b}}$, we end with the self-consistence condition

$$m_{\mathrm{b,eq}}[K, \mathrm{artanh}(m_{\mathrm{b}} \tanh K_{\mathrm{b}})] = m_{\mathrm{b}} \tag{15}$$

for the nonequilibrium order parameter m_{b}.

As $1 = \partial m_{\mathrm{b,eq}} / \partial m_{\mathrm{b}}|_{m_{\mathrm{b}}=0}$ at criticality, we obtain a very useful connection between the reduced zero-field boundary susceptibility of the equilibrium model $\chi^{(0)}_{\mathrm{b,eq}}(K) = \partial m_{\mathrm{b,eq}} / \partial h_{\mathrm{b}}|_{h_{\mathrm{b}}=0}$ and the critical temperature T_{c} of the driven system by expanding Eq. (15) to first order around $m_{\mathrm{b}} = 0$, namely,

$$\chi^{(0)}_{\mathrm{b,eq}}(K_{\mathrm{c}}) \tanh K_{\mathrm{b,c}} = 1. \tag{16}$$

In the following we will apply these results to the one- and two-dimensional models introduced in Sec. II.

C. 1d case

The effective Hamiltonian of the system 1d in a fluctuating field reads

$$\beta\mathcal{H} = -\sum_{l=1}^{L_\parallel} K\sigma_l\sigma_{l+1} + (h^{\mathrm{ext}} + K_{\mathrm{b}}\mu_l)\sigma_l. \tag{17}$$

Applying the self-consistence condition Eq. (15) to the well-known expression for the equilibrium magnetization of the one-dimensional (1D) Ising model (cf. [15])

$$m_{\mathrm{eq}}(K, h) = \frac{\sinh h}{\sqrt{e^{-4K} + \sinh^2 h}}, \tag{18}$$

we obtain the zero-field magnetization of the 1d driven system in the ordered phase for velocity $v \to \infty$,

$$m(K, K_{\mathrm{b}}) = \sqrt{\frac{\cosh 2K_{\mathrm{b}} - \coth 2K}{\cosh 2K_{\mathrm{b}} - 1}}, \tag{19}$$

with critical temperature fulfilling

$$e^{2K_c} \tanh K_{\mathrm{b,c}} = 1, \tag{20}$$

as $\chi^{(0)}_{\mathrm{eq}}(K) = e^{2K}$ in this case. Interestingly, Eq. (19) is equal to the spontaneous surface magnetization of the 2D equilibrium Ising model [[16], Chap. VI, Eq. 5.20] if we identify K and K_{b} with the couplings $\parallel$ and $\perp$ to the surface and consequently has the identical critical temperature T_{c}. For the special case $K = K_{\mathrm{b}}$ this gives the well-known value from Eq. (4). However, we regard this equality as coincidence without deeper meaning, as Eq. (19) is solution of a simple quadratic equation with small integer coefficients when written in the natural variables. Nevertheless, we checked this identity in the 2d case and found that we do *not* get the surface magnetization of the 3D system by the same procedure, as the critical temperature is $T_{\mathrm{c}} \approx 4.058$ [Eq. (60)] instead of the correct value $T_{\mathrm{c}} = 4.511\,424(53)$ [17,18].

To calculate other quantities we use the transfer-matrix (TM) formulation: the TM of the 1D equilibrium Ising model reads (cf. [52])

$$\mathbf{T}_{\mathrm{eq}} = \begin{pmatrix} e^{K+h} & e^{-K} \\ e^{-K} & e^{K-h} \end{pmatrix} \tag{21}$$

and the partition function of a periodic system with $L_\parallel$ spins can be expressed as

$$\mathcal{Z}_{\mathrm{eq}} = \mathrm{Tr}\, \mathbf{T}_{\mathrm{eq}}^{L_\parallel}. \tag{22}$$

Using Eq. (14) and the conditions Eq. (13) we can write

$$\mathcal{Z} = \mathrm{Tr}\ \mathbf{T}^{L_\parallel} \tag{23}$$

with the TM (we set $h^{\mathrm{ext}}=0$ from now on)

$$\mathbf{T} = \left.\frac{\cosh K_\mathrm{b}}{\cosh h}\mathbf{T}_{\mathrm{eq}}\right|_{\tanh h = m \tanh K_\mathrm{b}}, \tag{24}$$

which can be written as

$$\mathbf{T} = \cosh K_\mathrm{b}\begin{pmatrix} e^K(1+\sin\psi) & e^{-K}\cos\psi \\ e^{-K}\cos\psi & e^K(1-\sin\psi)\end{pmatrix} \tag{25}$$

using

$$\sin\psi = m\tanh K_\mathrm{b}. \tag{26}$$

The angle ψ decreases from $\psi=\pi/2$ at $T=0$ to $\psi=0$ at $T\geq T_\mathrm{c}$. The eigenvalues λ_μ of $\mathbf{T}$ fulfill

$$\mathbf{T}|t_\mu\rangle = \lambda_\mu|t_\mu\rangle \tag{27}$$

and are given by

$$\lambda_{0,1} = \begin{cases} e^{K\pm K_\mathrm{b}} & T\leq T_\mathrm{c} \\ \cosh K_\mathrm{b}(e^K \pm e^{-K}) & T\geq T_\mathrm{c}, \end{cases} \tag{28}$$

where λ_0 denotes the larger eigenvalue dominant in the thermodynamic limit. Note that in this limit the analog to the free-energy density

$$f = -\frac{1}{\beta}\ln\lambda_0 = -(J+J_\mathrm{b}) \tag{29}$$

of the driven system is simply a constant in the ordered phase $T\leq T_\mathrm{c}$ [35]. Nevertheless, we can calculate physical quantities within this TM notation using expectation values as the whole information of the half-infinite system is contained in the normalized eigenvectors

$$|t_0\rangle = \begin{pmatrix}\cos\phi \\ \sin\phi\end{pmatrix}, \quad |t_1\rangle = \begin{pmatrix}-\sin\phi \\ \cos\phi\end{pmatrix}, \tag{30}$$

with $\cos 2\phi = m$. Using the normalized TM $\hat{\mathbf{T}}=\mathbf{T}/\lambda_0$ and the Pauli matrix $\mathbf{M}=\mathrm{diag}(1,-1)$, the magnetization [Eq. (19)] can be expressed as

$$m = \langle t_0|\mathbf{M}|t_0\rangle, \tag{31}$$

while the correlation function in $\parallel$ direction becomes

$$\begin{aligned} g_\parallel(n) &= \langle\sigma_l\sigma_{l+n}\rangle - \langle\sigma_l\rangle\langle\sigma_{l+n}\rangle \\ &= \langle t_0|\mathbf{M}\hat{\mathbf{T}}^n\mathbf{M}|t_0\rangle - \langle t_0|\mathbf{M}|t_0\rangle^2 \\ &= \lambda_1^n\lambda_0^{-n}\langle t_0|\mathbf{M}|t_1\rangle^2, \end{aligned} \tag{32}$$

as $\mathbf{T}^n = \Sigma_\mu \lambda_\mu^n |t_\mu\rangle\langle t_\mu|$. We get the result

$$g_\parallel(n) = \begin{cases}(1-m^2)e^{-2nK_\mathrm{b}} & T\leq T_\mathrm{c} \\ \tanh^n K & T\geq T_\mathrm{c}, \end{cases} \tag{33}$$

leading to the inverse correlation length

$$\xi_\parallel^{-1} = \ln\frac{\lambda_0}{\lambda_1} = \begin{cases} 2K_\mathrm{b} & T\leq T_\mathrm{c} \\ \ln\coth K & T\geq T_\mathrm{c}. \end{cases} \tag{34}$$

Note that $\xi_\parallel$ does not diverge at the critical point, a feature which would lead to a correlation length exponent $\nu=0$. In Sec. IV we will argue that in finite systems the spin fluctuations are not only mediated by the spins σ_i but also by the self-consistent field m which fluctuates at finite $L_\parallel$, an effect which vanishes in the exact solution, as $L_\parallel\to\infty$.

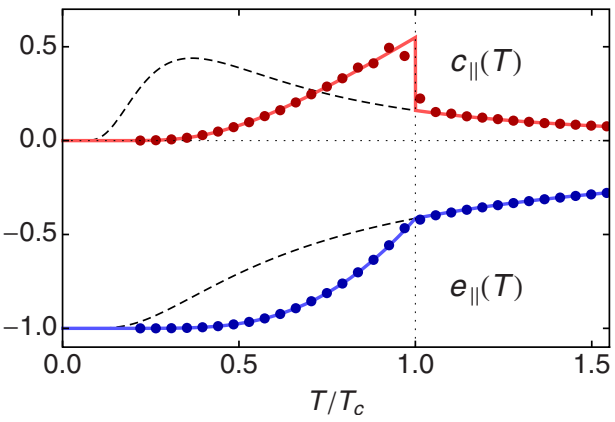

FIG. 5. (Color online) Internal energy $e_\parallel(T)$ [Eq. (35)] and specific heat $c_\parallel(T)$ [Eq. (36)] of the 1d driven system at $v\to\infty$. The points are MC results for $L_\parallel=2^{11}$, and the dashed lines are results for the one-dimensional Ising model in equilibrium.

From the nearest-neighbor correlation function we can calculate the internal energy $e_\parallel=-J\langle\sigma_l\sigma_{l+1}\rangle$ in $\parallel$ direction

$$e_\parallel = \begin{cases} \dfrac{Je^{-2K-K_\mathrm{b}}}{\sinh 2K\sinh K_\mathrm{b}} - 1 & T\leq T_\mathrm{c} \\ -J\tanh K & T\geq T_\mathrm{c} \end{cases} \tag{35}$$

as well as the specific heat $c_\parallel=\partial e_\parallel/\partial T$ in $\parallel$ direction (Fig. 5)

$$c_\parallel = \begin{cases} \dfrac{2K^2}{\sinh^2 K}(\coth K_\mathrm{b}-1) & T<T_\mathrm{c} \\ \dfrac{K^2}{\cosh^2 K} & T>T_\mathrm{c}. \end{cases} \tag{36}$$

On the other hand, the internal energy in $\perp$ direction is simply given by

$$e_\perp = -J_\mathrm{b}m^2 \tag{37}$$

as the related spins are uncorrelated.

Now we turn to dynamical properties of this system under a concrete MC Glauber dynamics (see Sec. IV B for details) and calculate the spin-flip acceptance rate $A=\langle p_{\mathrm{flip}}\rangle$ and the energy dissipation rate $P=\partial E/\partial t$: let $\langle\zeta_\ell\zeta\zeta_r\rangle$ denote the probability of picking a spin σ with direction $\zeta=\uparrow,\downarrow$ and left and right neighbors $\sigma_{\ell,r}$ with direction $\zeta_{\ell,r}$. These probabilities can be calculated using the matrices $\mathbf{P}_\uparrow=\mathrm{diag}(1,0)$ and $\mathbf{P}_\downarrow=\mathrm{diag}(0,1)$, e.g., $\langle\uparrow\uparrow\downarrow\rangle=\langle t_0|\mathbf{P}_\uparrow\hat{\mathbf{T}}\mathbf{P}_\uparrow\hat{\mathbf{T}}\mathbf{P}_\downarrow|t_0\rangle$. As the third coupling partner μ of spin σ, with direction ζ_μ, is uncorrelated at infinite velocity, the probability of a particular spin configuration becomes

$$\langle\zeta_\ell\zeta\zeta_r\rangle\langle\zeta_\mu\rangle = \langle t_0|\mathbf{P}_{\zeta_\ell}\hat{\mathbf{T}}\mathbf{P}_\zeta\hat{\mathbf{T}}\mathbf{P}_{\zeta_r}|t_0\rangle\langle t_0|\mathbf{P}_{\zeta_\mu}|t_0\rangle. \tag{38}$$

The spin-flip probability of a given configuration is $p_{\mathrm{flip}}(\Delta E)$, with $\Delta E=\Delta E_1+\Delta E_2=2J\sigma(\sigma_\ell+\sigma_r)+2J_\mathrm{b}\sigma\mu$, and A becomes the sum over all 2^4 possible cases

$$A = \sum_{\zeta_\ell,\zeta,\zeta_r,\zeta_\mu=\uparrow,\downarrow} p_{\text{flip}}(\Delta E)\langle\zeta_\ell\zeta\zeta_r\rangle\langle\zeta_\mu\rangle, \tag{39}$$

which can be written as

$$A = \sum_{\zeta_\ell,\zeta,\zeta_r=\uparrow,\downarrow} p^*_{\text{flip}}(\Delta E_1)\langle\zeta_\ell\zeta\zeta_r\rangle \sum_{\zeta_\mu=\uparrow,\downarrow} p^*_{\text{flip}}(\Delta E_2)\langle\zeta_\mu\rangle$$
$$= \sum_{\zeta=\uparrow,\downarrow} X_\zeta(e^{-2K_b}\langle\zeta\rangle + \langle\bar{\zeta}\rangle) \tag{40}$$

for the multiplicative rate $p^*_{\text{flip}}(\Delta E)=p^*_{\text{flip}}(\Delta E_1)p^*_{\text{flip}}(\Delta E_2)$ introduced in Sec. IV B [Eq. (69)] using the abbreviation

$$X_\zeta = \sum_{\zeta_\ell,\zeta_r=\uparrow,\downarrow} p^*_{\text{flip}}(\Delta E_1)\langle\zeta_\ell\zeta\zeta_r\rangle$$
$$= e^{-4K}\langle\zeta\zeta\zeta\rangle + 2e^{-2K}\langle\zeta\zeta\bar{\zeta}\rangle + \langle\bar{\zeta}\zeta\bar{\zeta}\rangle. \tag{41}$$

Note that the two terms in Eq. (40) are equal and the acceptance rate is independent of spin ζ because m is stationary. The resulting acceptance rate becomes

$$A = \begin{cases} \dfrac{\cosh(K+K_b)-\sinh(K-K_b)}{4e^{2(K+K_b)}\sinh K\cosh^2 K\sinh K_b} & T \le T_c \\ e^{-K_b}\cosh K_b(1-\tanh K)^2 & T \ge T_c, \end{cases} \tag{42}$$

which simplifies for $J=J_b$ to

$$A = \begin{cases} \dfrac{e^{-4K}\coth 2K}{\sinh 2K} & T \le T_c \\ \dfrac{e^{-3K}}{\cosh K} & T \ge T_c. \end{cases} \tag{43}$$

The calculation of the energy dissipation rate P per spin is very similar to the acceptance rate A [Eq. (40)] and gives

$$P = -2J_b \sum_{\zeta=\uparrow,\downarrow} X_\zeta(e^{-2K_b}\langle\zeta\rangle - \langle\bar{\zeta}\rangle). \tag{44}$$

Furthermore, P/A can be calculated for arbitrary dimensions and geometries, as it is solely a property of the fluctuating field. We find

$$\frac{P}{A} = -2J_b\frac{\Sigma_{\zeta=\uparrow,\downarrow}X_\zeta(e^{-2K_b}\langle\zeta\rangle - \langle\bar{\zeta}\rangle)}{\Sigma_{\zeta=\uparrow,\downarrow}X_\zeta(e^{-2K_b}\langle\zeta\rangle + \langle\bar{\zeta}\rangle)}$$
$$= -J_b\sum_{\zeta=\uparrow,\downarrow}\frac{e^{-2K_b}\langle\zeta\rangle - \langle\bar{\zeta}\rangle}{e^{-2K_b}\langle\zeta\rangle + \langle\bar{\zeta}\rangle}$$
$$= \frac{2J_b(m^2+1)\tanh K_b}{1-m^2\tanh^2 K_b}. \tag{45}$$

For the magnetization [Eq. (19)] of the 1d system this gives

$$\frac{P}{A} = \begin{cases} \dfrac{2J_b e^{-4K}}{\tanh K_b} & T \le T_c \\ 2J_b\tanh K_b & T \ge T_c, \end{cases} \tag{46}$$

which, multiplied with A from Eq. (71) and for $J=J_b$, becomes

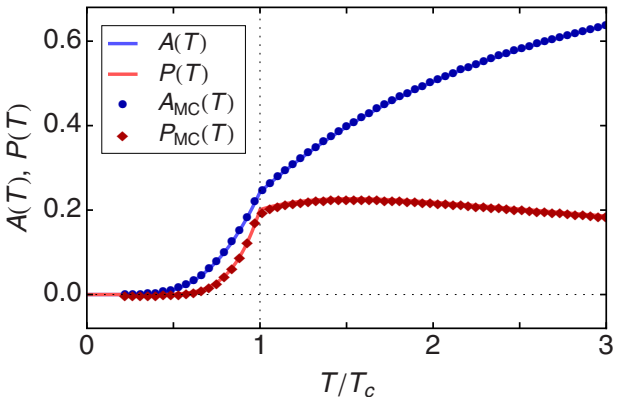

FIG. 6. (Color online) Spin-flip probability A [Eq. (43)] and energy dissipation rate P [Eq. (47)] versus reduced temperature T/T_c for the 1d system at $v\to\infty$, together with MC data for $L_\parallel=2^{11}$.

$$P = \begin{cases} \dfrac{2e^{-8K}\coth 2K}{\tanh K\sinh 2K} & T \le T_c \\ \dfrac{2e^{-3K}\tanh K}{\cosh K} & T \ge T_c. \end{cases} \tag{47}$$

These results are shown in Fig. 6, together with data from MC simulations. Note that these results are only valid for the multiplicative rate p^*_{flip} from Eq. (69).

Finally we list the critical exponents for the 1d driven system at $v\to\infty$ to be

$$\beta = \frac{1}{2}, \quad \gamma = 1, \quad \alpha = 0. \tag{48}$$

The behavior of this system at finite velocities v will be discussed in Sec. IV.

D. $2d_b$ case

The $2d_b$ case can be solved exactly using the expression for the equilibrium surface magnetization $m_{b,eq}(z,y_b)$ of the 2D Ising model in a static surface field h_b obtained by McCoy and Wu [[16], Chap. VI, Eq. 5.1], with $z=\tanh K$ and $y_b=\tanh h_b$. The integral representation given in their work can be further evaluated and written in closed form, the results are given in Appendix A [Eq. (A2)]. If we again use Eq. (15) and set $y_b=m_b z_b$, with $z_b=\tanh K_b$, we can calculate the nonequilibrium boundary magnetization $m_b(z,z_b)$ numerically as solution of the self-consistence condition

$$m_{b,eq}(z,m_b z_b) = m_b, \tag{49}$$

which is shown for $J=1$ and several values of J_b in Fig. 7. The critical temperature T_c of the system can be evaluated from the reduced zero-field boundary susceptibility $\chi_{b,eq}(z)$ [Eq. (A3)] to give

$$T_c = 2.661\ 472\ 565\ 575\ 2\ldots \tag{50}$$

for the case $J_b=J=1$ using $\chi^{(0)}_{b,eq}(z_c)z_{b,c}=1$ [Eq. (16)].

As the critical temperature T_c [Eq. (50)] is larger than the equilibrium critical temperature $T_{c,eq}=2.269\ 18\ldots$, the driven

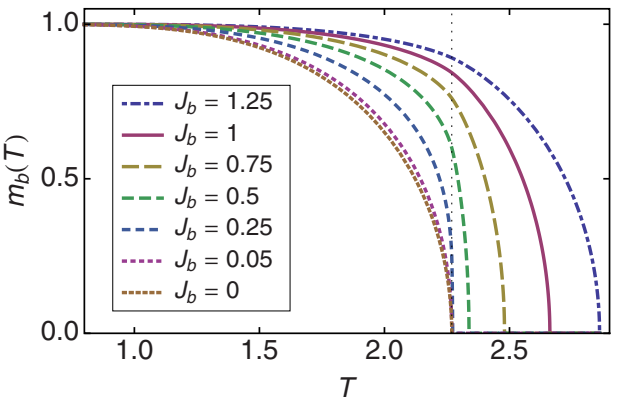

FIG. 7. (Color online) Boundary magnetization $m_b(T)$ [Eq. (49)] of the $2d_b$ system for $J=1$ and several values of J_b. For $J_b=0$ the m_b reduces to the surface magnetization of the 2D equilibrium Ising model [Eq. (A5)].

boundary induces a surface phase transition where only the driven surface has long range order above $T_{c,eq}$. The velocity dependence of this transition and the resulting phase diagram is discussed in more detail in Sec. IV.

E. 1+1d sheared case

If the motion of the lattice described by Eq. (3) is not restricted to one row but applied to the whole system, we get a system with uniform shear. Then all $\Delta_k(t) \equiv \Delta(t) = vt$ are equal, and we assume $K_{\perp,k} \equiv K_\perp$ to get

$$\beta\mathcal{H}(t) = -\sum_{k=1}^{L_\perp}\sum_{l=1}^{L_\parallel} K_\parallel \sigma_{k,l}\sigma_{k,l+1} + K_\perp \sigma_{k,l}\sigma_{k+1,l+\Delta(t)}. \quad (51)$$

Note that this system is translationally invariant in both directions, a fact that drastically simplifies the analysis of the critical behavior.

Now we will investigate this system in the limit $v \to \infty$. Then each spin σ_{kl} interacts, as depicted in Fig. 8, with its neighbors $\sigma_{k\pm1,l\pm\Delta(t)}$ via fluctuating fields, while the interaction to the parallel neighbors $\sigma_{k,l\pm1}$ remains unchanged. Thus the system decomposes into $L_\perp$ identical 1D Ising models which again can be solved exactly: the coupling to two fluctuating fields $\mu_{i,1}$ and $\mu_{i,2}$ with equal strength k_i on each site can be traced similar to Eq. (10) to give

$$\begin{aligned}\mathcal{Z} &= \mathrm{Tr}_\sigma\, e^{-\beta\mathcal{H}_0}\, \mathrm{Tr}_\mu \prod_i \prod_{j=1}^{2} e^{k_i \mu_{ij}\sigma_i} \\ &= \mathrm{Tr}_\sigma\, e^{-\beta\mathcal{H}_0} \prod_i \prod_{j=1}^{2} \sum_{\mu_{ij}=\pm1} e^{k_i\mu_{ij}\sigma_i} p_i(\mu_{ij}) \\ &= \mathrm{Tr}_\sigma\, e^{-\beta\mathcal{H}_0} \prod_i [\cosh k_i + m_i\sigma_i \sinh k_i]^2 \\ &= \prod_i C_i\, \mathrm{Tr}_\sigma\, e^{-\beta\mathcal{H}_0} \prod_i \left[1 + \sigma_i \frac{m_i}{C_i} \sinh 2k_i\right], \end{aligned} \quad (52)$$

with

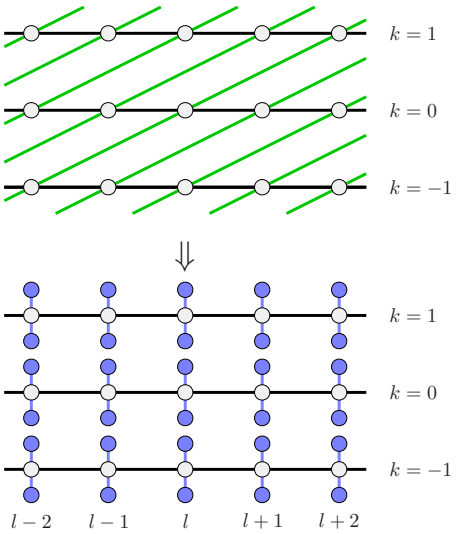

FIG. 8. (Color online) Mapping of the 1+1d sheared system, shown for $\Delta=2$, on $L_\perp$ disconnected 1D systems with fluctuating fields.

$$C_i = \frac{1}{2}(1 - m_i^2 + (1 + m_i^2)\cosh 2k_i). \quad (53)$$

Equating Eq. (52) with Eq. (12) we conclude that static fields b_i can replace the fluctuating fields μ_{ij}, with average m_i, if

$$\tanh b_i = \frac{2m_i \sinh 2k_i}{1 - m_i^2 + (1 + m_i^2)\cosh 2k_i}. \quad (54)$$

The sheared system is translationally invariant in both directions, leading to homogeneous values $m_i=m$, $k_i=K_\perp$, and $b_i=h$. Inserting Eq. (54) into Eq. (19) we get the order parameter of the sheared 1+1d system

$$m(K_\parallel, K_\perp) = \frac{\sqrt{1 - 2e^{4K_\parallel} + 2e^{2K_\parallel}\sqrt{e^{4K_\parallel} - 1 + \tanh^2 K_\perp}}}{\tanh K_\perp}, \quad (55)$$

with critical temperature fulfilling

$$2e^{2K_{\parallel,c}} \tanh K_{\perp,c} = 1, \quad (56)$$

which gives $T_c = 1/\ln(\frac{1}{2}\sqrt{3+\sqrt{17}}) = 3.465\,91\ldots$ for $J_\parallel = J_\perp = 1$. A generalization of Eq. (52) from two to f fluctuating fields per spin is straightforward and leads to the general criticality condition

$$\chi_{eq}^{(0)}(K_c) f \tanh K_{b,c} = 1. \quad (57)$$

Although this geometry can be solved exactly at $v=\infty$ we expect the phase transition to be *strongly anisotropic* (see, e.g., [19]) with two different correlation length exponents $\nu_\parallel > \nu_\perp$. In fact we found such behavior, with strong evidence for the exponents $\nu_\parallel = 3/2$ and $\nu_\perp = 1/2$, details on this will be published elsewhere [20].

F. Other geometries

For two more cases we can derive highly accurate estimates for the critical temperature T_c of the driven system

when $v \to \infty$, namely, the 2d Ising double layer [20] with Hamiltonian

$$\beta\mathcal{H}(t) = -\sum_{k=0}^{1}\sum_{l=1}^{L_\parallel}\sum_{m=1}^{L_\parallel}[K\sigma_{klm}(\sigma_{k,l,m+1}+\sigma_{k,l+1,m}) + K_b\sigma_{0lm}\sigma_{1,l+\Delta(t),m}] \tag{58}$$

and the experimentally relevant 2+1d sheared case

$$\beta\mathcal{H}(t) = -\sum_{k=1}^{L_\perp}\sum_{l=1}^{L_\parallel}\sum_{m=1}^{L_\parallel}[K_\parallel\sigma_{klm}(\sigma_{k,l,m+1}+\sigma_{k,l+1,m}) + K_\perp\sigma_{klm}\sigma_{k+1,l+\Delta(t),m}], \tag{59}$$

both on simple cubic lattices: with Eq. (57) we can express T_c using the high-temperature series expansion for the reduced zero-field susceptibility $\chi_{eq}^{(0)}(K)$ of the 2D Ising model, which was calculated to higher than 2000th order recently using a highly efficient polynomial time algorithm [21]. Using this extremely accurate result we find, for $J=J_b=1$, the critical temperatures

$$T_c = 4.058\ 782\ 423\ 137\ 980\ 000\ 987\ 775\ 040\ 680\ldots \tag{60}$$

for the two 2d layers and

$$T_c = 5.264\ 750\ 414\ 514\ 743\ 550\ 598\ 017\ 203\ 424\ldots \tag{61}$$

for the 2+1d sheared system with $f=2$ analogous to the 1+1d sheared system. Note that due to the high accuracy of the series these values can be calculated to approximately 500 and 700 digits, respectively.

Just for reference we also give the critical temperatures for two more cases: the experimentally relevant $3d_b$ case shown in Fig. 1 as well as the quite theoretical 3d case of two three-dimensional systems in direct contact along the fourth dimension. In the $3d_b$ case we find $T_c=4.8(1)$ using the eighth-order high-temperature series from Ref. [22] (Table IV), while in the 3d case we obtain $T_c=5.983\ 835(1)$ using the 32th order series from [23].

All these higher-dimensional geometries are expected to show strongly anisotropic behavior with two different correlation length exponents, the reader is referred to Ref. [20].

IV. MONTE CARLO SIMULATIONS

A. Method

We now describe the algorithms used to investigate the driven system: for finite velocities v we shift the boundary couplings by increasing $\Delta(t)$ from Eq. (2) after every N/v random sequential single spin-flip attempts, where N denotes the total number of spins. Using 10^5–10^6 MCS per temperature, we measured the following boundary properties: the boundary magnetization per spin and the energy per bond parallel to and across the boundary of a given configuration

$$M_b = \frac{1}{2L_\parallel}\sum_{k=0}^{1}\sum_{l=1}^{L_\parallel}\sigma_{k,l}, \tag{62a}$$

$$E_{b,\parallel} = -\frac{J}{2L_\parallel}\sum_{k=0}^{1}\sum_{l=1}^{L_\parallel}\sigma_{k,l}\sigma_{k,l+1}, \tag{62b}$$

$$E_b = -\frac{J_b}{L_\parallel}\sum_{l=1}^{L_\parallel}\sigma_{0,l}\sigma_{1,l+\Delta(t)}, \tag{62c}$$

as well as the corresponding bulk quantities. From these time-dependent quantities we calculate the averages of the magnetization, reduced susceptibility, Binder cumulant, internal energy, and specific heat at the boundary,

$$m_{b,abs} = \langle|M_b|\rangle, \tag{63a}$$

$$\chi_{b,abs} = 2L_\parallel(\langle M_b^2\rangle - \langle|M_b|\rangle^2), \tag{63b}$$

$$U_b = 1 - \frac{\langle M_b^4\rangle}{3\langle M_b^2\rangle^2}, \tag{63c}$$

$$e_b = \langle E_b\rangle, \tag{63d}$$

$$c_b = L_\parallel\beta^2(\langle E_b^2\rangle - \langle E_b\rangle^2). \tag{63e}$$

Note that we have absorbed the factor β^{-1} into χ. Near criticality these quantities show power-law behavior and fulfill

$$m_{b,abs}(\tau) \propto (-\tau)^\beta, \tag{64a}$$

$$\chi_{b,abs}(\tau) \propto |\tau|^{-\gamma}, \tag{64b}$$

$$c_b(\tau) \propto |\tau|^{-\alpha}, \tag{64c}$$

with reduced temperature $\tau=T/T_c-1$ and critical exponents β, γ, and α. But before we present the results, we have to take a closer look at the used spin-flip rates.

B. Integrable algorithm

While equilibrium properties are most efficiently investigated in Monte Carlo simulations using cluster algorithms, nonequilibrium systems have to be treated with random sequential single spin-flip dynamics such as the nonconserved Glauber dynamics [24] or the conserved Kawasaki dynamics [25]. The driven system is permanently under an external perturbation which drives it out of equilibrium, while the internal degrees of freedom are coupled to a heat bath in thermal equilibrium. From this coupling the spin-flip probability $p_{flip}(\Delta E)$ of a given energy change ΔE fulfills the detailed balance condition

$$\frac{p_{flip}(\Delta E)}{p_{flip}(-\Delta E)} = e^{-\beta\Delta E}, \tag{65}$$

just like in the equilibrium case (for details, see [20]).

The most common rates fulfilling Eq. (65) are the Metropolis rate [26] and the Glauber rate [24],

$$p_{flip}^M(\Delta E) = \min(1, e^{-\beta\Delta E}), \tag{66a}$$

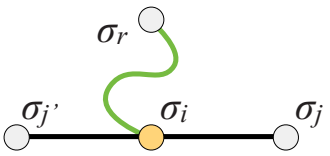

FIG. 9. (Color online) Interactions of surface spin σ_i in the 1d case.

$$p^{\mathrm{G}}_{\mathrm{flip}}(\Delta E) = \frac{1}{1 + e^{\beta \Delta E}}. \tag{66b}$$

Using these rates in simulations of, e.g., the 1d driven system [Eq. (1)], it turns out that for all $v > 0$ the critical temperature $T_c(v)$ depends on the used rate (see also Fig. 15): we find, for $v \to \infty$ and $J_b = J = 1$, the values $T_c^{\mathrm{M}} = 1.910(2)$ and $T_c^{\mathrm{G}} = 2.031(2)$ for the Metropolis and Glauber rate, respectively, while the exact solution [Eq. (20)] of the model presented in Sec. III gives $T_c = 2.269\ldots$. Note that a similar dependency was recently found in the DLG by Kwak *et al.* [27].

How can these discrepancies be understood? And can we construct a rate that matches the analytical treatment, i.e., has the same T_c? This is indeed possible: consider a microscopic change, i.e., a spin flip, of spin σ_i at the boundary (see Fig. 9) with energy difference

$$\Delta E = \underbrace{2J\sigma_i \sum_{\langle j \rangle}^{z} \sigma_j}_{\Delta E_1} + \underbrace{2J_b \sigma_i \sigma_r}_{\Delta E_2}, \tag{67}$$

where the sum runs over the z neighbors of σ_i in the same subsystem ($z = 2$ in the 1d case), while σ_r is from the other side of the moving boundary. The idea of the exact solution presented in the last section was to treat spin σ_r as a fluctuating variable μ_i at site i with appropriate statistics. By contrast, correlations of different strength are introduced between the two subsystems by the rates [Eq. (65)] because the influence of spin σ_r depends on the actual state of the z spins σ_j. This can be seen most easily in the case of the Metropolis rate ($J_b = J$): if, e.g., $\sigma_i = -\sigma_j$ then $\Delta E_1 = -2zJ$ and $p^{\mathrm{M}}_{\mathrm{flip}} = 1$ independent of σ_r (note that $\Delta E_2 = \pm 2J$), while in the parallel case ($\sigma_i = \sigma_j$) $\Delta E_1 = 2zJ$ and $p^{\mathrm{M}}_{\mathrm{flip}}$ strongly depends on σ_r (see Fig. 10).

Fortunately, these rate-induced correlations can be completely eliminated by requiring that *the flipping probability is multiplicative*,

$$p_{\mathrm{flip}}(\Delta E_1 + \Delta E_2) = p_{\mathrm{flip}}(\Delta E_1) p_{\mathrm{flip}}(\Delta E_2). \tag{68}$$

Clearly this condition is not satisfied for the rates in Eq. (65), e.g., $p^{\mathrm{M}}_{\mathrm{flip}}(-2zJ + 2J) = 1$, while $p^{\mathrm{M}}_{\mathrm{flip}}(-2zJ) p^{\mathrm{M}}_{\mathrm{flip}}(2J) = e^{-2K}$ (again we assume $J_b = J$).

Instead, for simulations of driven systems we propose the rate

$$p^{*}_{\mathrm{flip}}(\Delta E) = e^{-\beta/2(\Delta E - \Delta E_{\mathrm{min}})}, \tag{69}$$

which is uniquely defined by the detailed balance condition [Eq. (65)] and the multiplicity condition [Eq. (68)] [36]. The constant ΔE_{min} is the minimum possible value of ΔE at given geometry; this assures that $p^{*}_{\mathrm{flip}}(\Delta E)$ is maximal but never larger than one. For our example [Eq. (67)] we find $\Delta E_{1,\mathrm{min}} = -2zJ$ and $\Delta E_{2,\mathrm{min}} = -2J_b$ to fulfill Eq. (68). This rate reproduces the calculated critical temperatures in all considered geometries, e.g., $T_c^{*} = 2.269(1)$ for the 1d case at $v \to \infty$.

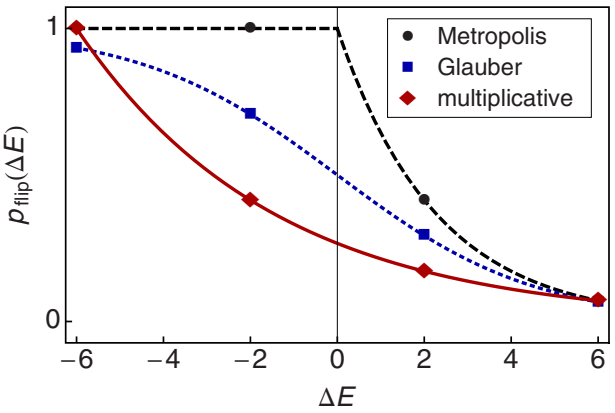

FIG. 10. (Color online) Spin-flip probabilities of the Metropolis rate [Eq. (66a)] (dashed black line, circles), the Glauber rate [Eq. (66b)] (dotted blue line, squares), and the multiplicative rate [Eq. (69)] (red line, diamonds) for the 1d system at criticality ($J = J_b = 1$).

The resulting spin-flip rates for the 1d case at criticality are shown in Fig. 10. Clearly, the multiplicative algorithm [Eq. (69)] has a smaller overall acceptance rate than Eqs. (66) and is thus slightly less efficient: a finite-size scaling analysis of the acceptance rate $A = \langle p_{\mathrm{flip}} \rangle$ at criticality in the 1d case yields $A_c^{\mathrm{M}} = 0.476(2)$, $A_c^{\mathrm{G}} = 0.366(2)$ and $A_c^{*} = 0.242(2)$ for the three algorithms, rendering this method roughly two times slower than the Metropolis algorithm. In fact, $A_c = 3\sqrt{2} - 4 = 0.242\,64\ldots$ can be calculated exactly from Eq. (43).

Note that the Metropolis and Glauber rates can be considered as many particle rates, as p_{flip} depends on the many particle state of all coupling partners, while the multiplicative rate corresponds to a product of two particle contributions. We believe that the dynamics generated by the multiplicative rate is generally simpler than the one generated by Metropolis or Glauber rates, making an exact solution more feasible. Whether this differentiation only holds for the nonconserved Glauber dynamics or also for the conserved Kawasaki dynamics is subject of future work.

In the next two sections we will investigate finite-size effects in the 1d case as well as the crossover behavior at finite velocities v in the 1d as well as in the $2d_b$ case. We first turn to the 1d case.

C. 1d case

The exact solution presented in Sec. III was derived in the thermodynamic limit $L_{\parallel} \to \infty$ as we assumed a constant and nonfluctuating order parameter m in the self-consistence condition [Eq. (15)]. This led to the result that the correlation length $\xi_{\parallel}$ [Eq. (34)] remains finite at criticality. However, in a finite system the assumption $m = \mathrm{const}$ is not fulfilled and finite-size effects occur, leading to a nontrivial dependency

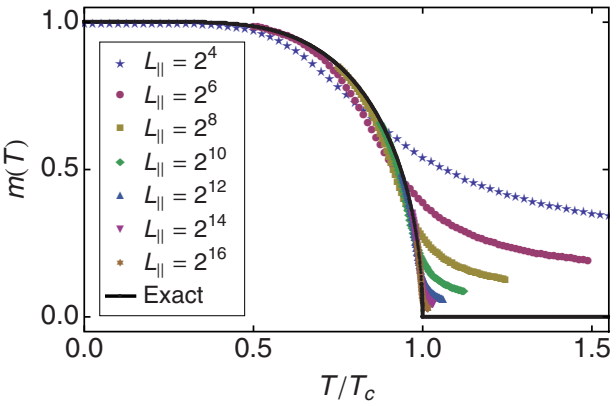

FIG. 11. (Color online) Magnetization $m_{\mathrm{abs}}(T)$ [Eq. (64a)] of the 1d system at $v=\infty$ for several system sizes $L_\parallel$ from Monte Carlo simulations, together with the exact solution Eq. (19).

of the physical quantities on system size. The fluctuating order parameter gives rise to additional correlations between spins at large distances not included in the exact solution. As the driven system shows mean-field behavior, we can use the standard finite-size scaling theory for mean-field systems: near criticality the correlation length parallel to the boundary fulfills $\xi_\parallel(\tau) \propto |\tau|^{-\nu_\parallel}$ with critical exponent $\nu_\parallel = 2/\mathrm{d_b}$, where $\mathrm{d_b}$ denotes the boundary dimension. We have $\mathrm{d_b}=1$ in both the 1d and the $2\mathrm{d_b}$ case, leading to $\nu_\parallel=2$ in these cases.

To illustrate these finite-size effects in the 1d case, in Fig. 11 we show the magnetization $m_{\mathrm{abs}}(T)$ [Eq. (64a)] as function of temperature for $v=\infty$ and several system sizes $L_\parallel$. The exact solution [Eq. (19)] is only approached in the limit $L_\parallel \to \infty$.

The finite-size scaling behavior is demonstrated exemplarily for the susceptibility $\chi_{\mathrm{abs}}(T)$ [Eq. (64b)], which is shown in a finite–size scaling plot in Fig. 12: after rescalation of the MC data in the usual way we indeed find the expected mean-field exponents $\gamma=1$ and $\nu_\parallel=2$, furthermore the data falls onto the universal finite-size scaling function calculated in Ref. [28]. The same analysis was performed for

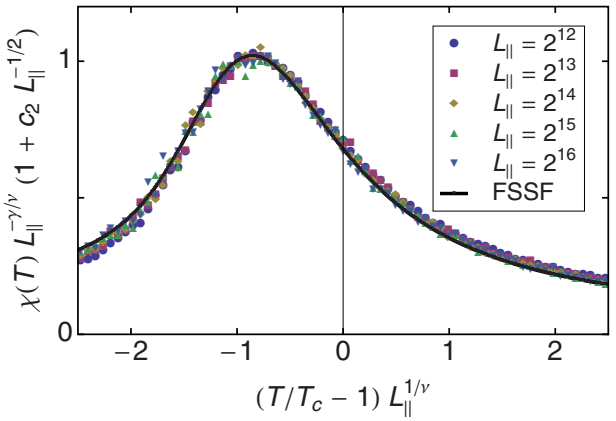

FIG. 12. (Color online) Finite-size scaling plot of the reduced susceptibility $\chi_{\mathrm{abs}}(T)$ [Eq. (64b)] of the 1d system for $v=\infty$ and system sizes $L_\parallel = 2^{12}, \ldots, 2^{16}$, together with the exact mean-field finite-size scaling function (black line) from Ref. [28]. The correction factor $c_2=2.7$.

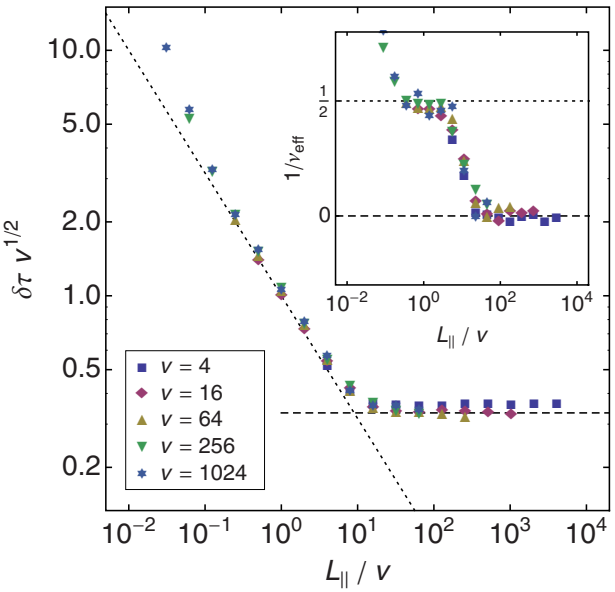

FIG. 13. (Color online) Velocity dependent crossover behavior in the 1d case. Shown is the rescaled width of the critical region $\delta\tau v^{1/2}$ as function of the crossover scaling variable $L_\parallel/v$ for several velocities v and several system sizes $L_\parallel = 2^4, \ldots, 2^{16}$ (see text). The inset shows the corresponding crossover of the effective correlation length exponent ν_{eff}^{-1} from $\nu_{\mathrm{eff}}^{-1}=1/2$ (MF, dotted line) to $\nu_{\mathrm{eff}}^{-1}=0$ (Ising noncritical, dashed line).

the magnetization $m_{\mathrm{abs}}(T)$ and specific heat $c(T)$ [Eq. (64c)], verifying the other two exponents $\beta=1/2$ and $\alpha=0$.

In summary, the 1d and the $2\mathrm{d_b}$ systems with boundary dimension $\mathrm{d_b}=1$ have the standard mean-field exponents and fulfill the exponent relations

$$2 - \alpha = 2\beta + \gamma = \mathrm{d_b}\nu_\parallel. \tag{70}$$

We now turn to finite velocities v: then the 1d system always shows a crossover from mean field to Ising behavior with increasing system size $L_\parallel$. Only in the limit $v \to \infty$ the system undergoes a phase transition at finite temperatures. To investigate this velocity-dependent crossover, we measured the width $\delta\tau$ of the critical region by analyzing the Binder cumulant [Eq. (63c)]. Using least-squares fits of the simulation data to the simple approximation,

$$U_{\mathrm{b}}(T) \approx \begin{cases} \frac{1}{3}[1 + \tanh(\tilde{\tau}/\delta\tau)] & \tilde{\tau} \le 0 \\ \frac{1}{3}\frac{1}{1 + \tilde{\tau}/\delta\tau} & \tilde{\tau} > 0, \end{cases} \tag{71}$$

with $\tilde{\tau} = T/\tilde{T}_{\mathrm{c}} - 1$ and fit parameters $\tilde{T}_{\mathrm{c}}$ and $\delta\tau$, for several velocities v and system sizes $L_\parallel$ we determined $\delta\tau$ and plotted them in Fig. 13. We find that the crossover scaling variable is $L_\parallel/v$ in this case, while the y axis has to be rescaled as $\delta\tau v^{1/2}$ to get the correct limit $L_\parallel^{1/\nu_\parallel}\delta\tau = \mathrm{const}$ with $\nu_\parallel=2$ in the limit $v \to \infty$. At finite v the width $\delta\tau$ stops shrinking at $L_\parallel^\times \approx 9v$, where $L_\parallel^\times$ denotes the crossover system size, and only goes to zero for $v \to \infty$, indicating a sharp phase transition in this limit. The inset shows the effective exponent ν_{eff} obtained from the logarithmic derivative,

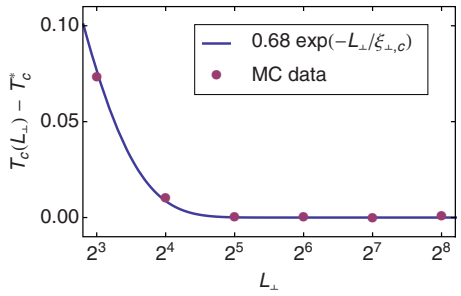

FIG. 14. (Color online) Influence of the system size $L_\perp$ on the critical point in the $2d_b$ case at $v=\infty$ and $L_\parallel=256$. The effective critical temperature $T_c(L_\perp)$ shifts to higher values if $L_\perp \lesssim 10\xi_{\perp,c}$ (see text).

$$\nu_{\text{eff}}^{-1} = -\frac{\partial \ln \delta\tau}{\partial \ln L_\parallel}, \tag{72}$$

whose value changes from $\nu_{\text{eff}}^{-1}=1/2$ (MF) to $\nu_{\text{eff}}^{-1}=0$ (Ising) with growing system size. In the next section we will see that this behavior changes substantially in the $2d_b$ case.

D. $2d_b$ case

In the $2d_b$ case the moving boundary is coupled to a two-dimensional Ising model, which undergoes a phase transition at $T_{c,eq}$ [Eq. (4)], independent of the velocity v. In addition, the moving boundary shows a boundary phase transition at temperature $T_c(v)$, which grows with increasing v and eventually approaches the value given in Eq. (50) for $v\to\infty$. As $T_c(v)>T_{c,eq}$ for all $v>0$ we expect a boundary phase transition with paramagnetic bulk. Then the correlation length $\xi_\perp$ perpendicular to the boundary is finite at criticality and has the Ising value

$$\xi_{\perp,c}(v) = \xi_{eq}[T_c(v)], \tag{73}$$

with [16]

$$\xi_{eq}^{-1}(T) = \begin{cases} 4K - 2\ln\coth K & T < T_{c,eq} \\ \ln\coth K - 2K & T > T_{c,eq}. \end{cases} \tag{74}$$

For that reason, in the finite-size scaling analysis it is sufficient for given v to simulate systems with varying length $L_\parallel$ while holding the height $L_\perp$ fixed at a value $L_\perp \gg \xi_{\perp,c}(v)$. To illustrate this behavior, in Fig. 14 we show the effect of different values of $L_\perp$ for $v=\infty$ and $L_\parallel=256$. Only below $L_\perp \approx 32$ the system feels the finite width $L_\perp$, resulting in a shift of the effective critical temperature $T_c(L_\perp)$ to higher values. The strength of the shift is proportional to the correlation function in $\perp$ direction, $\langle \sigma_{0,l}\sigma_{L_\perp,l}\rangle \propto \exp(-L_\perp/\xi_{\perp,c})$. The curves collapse for $L_\perp>32$ showing that a ratio $L_\perp/\xi_{\perp,c}\approx 10$ is sufficient as $\xi_{\perp,c}(\infty)=3.663\,23\ldots$ in this case.

We performed MC simulations and determined the critical temperatures for different velocities v by performing a finite-size scaling analysis of the boundary susceptibility $\chi_{\text{abs,b}}(T)$ and the boundary cumulant $U_b(T)$. For the multiplicative algorithm, Eq. (69), we used 400.000 MC steps per temperature, while for the Metropolis algorithm 50.000 MC steps per temperature were used. The results are given in Table I and are compiled into a phase diagram of the $2d_b$ case shown in Fig. 15. An important aspect of this phase diagram is the possibility of a velocity driven nonequilibrium phase transition at fixed temperature (double arrow): while the system is paramagnetic at $v=0$ and up to $v_c(T)$ (thick blue line), the boundary shows long range order above that velocity. It would be interesting to see this transition in experiments, which could be performed in the corresponding geometry $3d_b$ (see Fig. 1), e.g., using two close rotating magnets slightly above the Curie temperature. The magnets should be isolating to avoid eddy currents [4].

TABLE I. Velocity dependent critical temperatures $T_c(v)$ for the $2d_b$ case, estimated using the multiplicative rate, [Eq. (69)] with 400.000 MC sweeps per temperature as well as using the Metropolis rate [Eq. (66a)] with 50.000 MC sweeps per temperature.

v	$T_c^*(v)$	$T_c^M(v)$
1/16	2.301(2)	
1/4	2.33(1)	
1	2.41(1)	2.30(2)
4	2.52(1)	2.37(2)
16	2.61(1)	2.42(2)
64	2.644(3)	2.44(2)
256	2.654(2)	2.44(2)
1024	2.659(2)	2.45(2)
∞	2.661(1)	2.45(2)

In the $2d_b$ case the crossover scaling variable can be determined from the $T_c(v)$ dependency discussed above. The correlation length ξ_{eq} at the critical point of the driven sys-

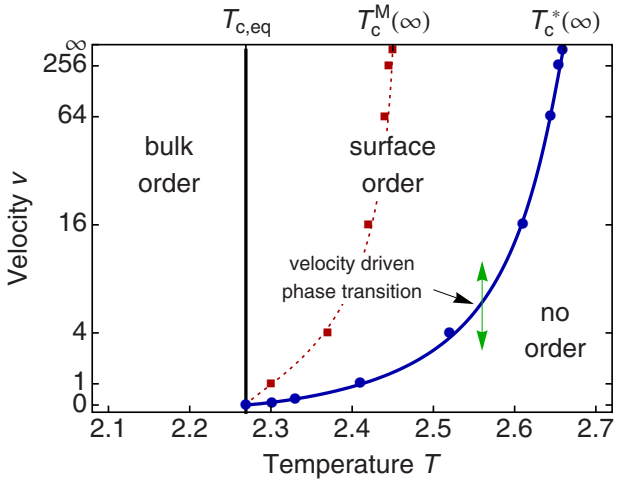

FIG. 15. (Color online) Phase diagram of the $2d_b$ case. Below $T_{c,eq}$ the two-dimensional bulk is ordered, while surface order is observed even above $T_{c,eq}$ up to the velocity dependent phase boundary $T_c(v)$. The position of this boundary depends on the algorithm, the blue line holds for the multiplicative rate [Eq. (69)], while the thin red dotted line holds for the Metropolis rate [Eq. (66a)]. At fixed temperatures between $T_{c,eq}$ and $T_c(v)$ a velocity driven phase transition is possible. The points are results from MC simulations.

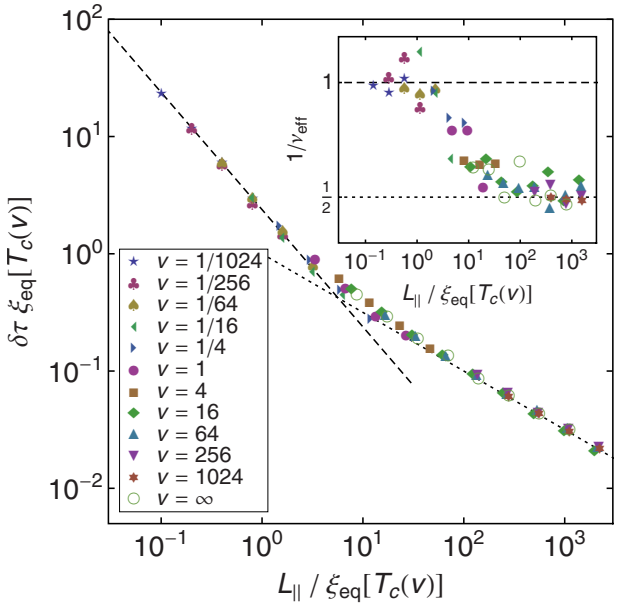

FIG. 16. (Color online) Velocity dependent crossover behavior in the $2d_b$ case. Shown is the rescaled width of the critical region $\delta\tau\xi_{eq}[T_c(v)]$ as function of the crossover scaling variable $L_\parallel/\xi_{eq}[T_c(v)]$ for several velocities v and different system sizes $L_\parallel=2^4,\ldots,2^{10}$ (see text). The inset shows the corresponding crossover of the effective correlation length exponent ν_{eff} from $\nu_{eff}=1$ (Ising, dashed line) to $\nu_{eff}=2$ (MF, dotted line).

tem, $T_c(v)$, plays a key role: The system is Ising-like as long as correlations span the whole system in both directions $\parallel$ and $\perp$, i.e., as long as the system size $L_\parallel$ is of the order of the bulk correlation length ξ_{eq} at the critical point $T_c(v)$ of the driven system, leading to the crossover scaling variable $L_\parallel/\xi_{eq}[T_c(v)]$. Again, the rescaling of the y axis can be determined by requiring that a data collapse is obtained in the limit $v\to 0$, leading to the expression $\delta\tau\xi_{eq}[T_c(v)]$, as ξ_{eq} cancels in this case and we get the required condition $L_\parallel\delta\tau=$const, as $\xi_{eq}\propto\tau^{-\nu_{eq}}$ in this limit and $\nu_{eq}=1$.

The resulting crossover scaling plot is shown in Fig. 16. For all finite $v>0$ the critical behavior changes from Ising to mean field at the crossover system size $L_\parallel^\times\approx 6\xi_{eq}[T_c(v)]$: below this value $\delta\tau$ shrinks according to $\delta\tau\propto L_\parallel^{-1}$ (Ising, dashed line), while above this value $\delta\tau\propto L_\parallel^{-1/2}$ holds (MF, dotted line). As the shift exponent θ at small velocities defined by

$$T_c(v)-T_c(0)\propto v^\theta \tag{75}$$

is close to 1/2 we have, for small v, $L_\parallel^\times\propto v^{-\theta}\approx v^{-1/2}$. The shift exponent $\theta=1/2$ has also been found in a field theoretical calculation of the 2+1d system [29].

V. SUMMARY

In this work we investigated a recently proposed driven Ising model with friction due to magnetic correlations. The nonequilibrium phase transition present in this system was investigated in detail using analytical methods and Monte Carlo simulations. In the far from equilibrium limit of high driving velocities $v\to\infty$ the model was solved exactly by integrating out the nonequilibrium degrees of freedom. The resulting exact self-consistence equation was analyzed for various geometries, leading in many cases to precise values of the critical temperature T_c of the nonequilibrium phase transition. In the limit $v\to\infty$ the system always shows mean-field behavior due to dimensional reduction independent of geometry. In the simplest one-dimensional case denoted 1d a complete analysis of both equilibrium as well as nonequilibrium quantities has been presented. These exact results are another example of mean-field critical behavior in an exactly solvable driven system, just as in the case of the DLG in a certain limit [30].

The analytic results were reproduced using a multiplicative Monte Carlo rate originally introduced in [30], which eliminates correlations due to many particle dynamics introduced by the common Metropolis and Glauber rates. We claim that this algorithm is generally favorable to the Metropolis and Glauber rates if an analytical treatment is considered.

The finite-size effects naturally emerging in the simulations were analyzed using finite-size scaling techniques, a perfect agreement with exactly known universal finite-size scaling functions [28] were found.

We analyzed the critical behavior at finite velocities and studied the crossover behavior from low to high velocities: we found that the 1d system only has a phase transition in the thermodynamic limit for $v=\infty$, while systems with finite v always become noncritical at the crossover system size $L_\parallel^\times\approx 9v$. On the contrary, the two-dimensional case $2d_b$ already has an Ising type phase transition at $v=0$, which changes to mean-field behavior for *all* finite $v>0$ in the thermodynamic limit, at a crossover length $L_\parallel^\times\approx 6\xi_{eq}[T_c(v)]$. In this sense, the velocity v is a relevant perturbation, always driving the system to a nonequilibrium state.

The 1d system changes from mean field to noncritical Ising universality, while the $2d_b$ case changes from Ising to mean-field type with growing system size $L_\parallel$. This somewhat puzzling fact can be understood in terms of the critical width $\delta\tau$ of the transition as follows: as in general $\delta\tau\propto L_\parallel^{-1/\nu}$ at criticality, in the two-dimensional Ising case $\delta\tau\propto L_\parallel^{-1}$, while in the mean-field case with one-dimensional boundary $\delta\tau\propto L_\parallel^{-1/2}$. Third, $\delta\tau\propto L_\parallel^0=$const in the 1d case at finite v. In the crossover the actual critical width $\delta\tau$ is always governed by the largest contribution and so at sufficiently large system size $L_\parallel$ the contribution with smallest ν^{-1} dominates and determines the critical behavior. As consequence in both cases the effective inverse correlation length exponent ν_{eff}^{-1} changes from a larger value at small $L_\parallel$ to a smaller value at large $L_\parallel$ ($1/2\to 0$ in the 1d case, $1\to 1/2$ in the $2d_b$ case).

Comparing the results to the driven lattice gas (DLG) [10], we note that the DLG also shows a continuous nonequilibrium phase transition from an ordered to a disordered state at a critical temperature which grows with growing driving field. However, in the DLG the particle number is conserved, while we deal with a nonconserved magnetization.

Finally some remarks on strongly anisotropic critical behavior: the sheared system denoted 1+1d shows strongly anisotropic behavior at criticality and $v\to\infty$, with strong evidence for the correlation length exponents $\nu_\parallel=3/2$ and $\nu_\perp$

$=1/2$, details on this will be published elsewhere [20]. Remarkably, this is a rare case of an exactly solvable nonequilibrium system with strongly anisotropic critical behavior.

ACKNOWLEDGMENTS

Special thanks go to Dietrich E. Wolf for very valuable discussions, criticism, and comments within the framework of the Sonderforschungsbereich 616, "Energy Dissipation at Surfaces." Thanks also to Sebastian Angst, Lothar Brendel, and Felix Schmidt for helpful discussions and to Sven Lübeck for critical reading of the paper.

APPENDIX A: SURFACE MAGNETIZATION OF THE 2D ISING MODEL

The equilibrium surface magnetization $m_{\mathrm{b,eq}}$ of the 2D Ising model in a static surface field h_{b} obtained by McCoy and Wu ([16], Chapter VI, Eq. 5.1) as well as the reduced zero-field boundary susceptibility

$$\chi_{\mathrm{b,eq}}^{(0)} = \left.\frac{\partial m_{\mathrm{b,eq}}}{\partial h_{\mathrm{b}}}\right|_{h_{\mathrm{b}}\to 0} \tag{A1}$$

can be written in closed form not present in the literature yet [31]. $\chi_{\mathrm{b,eq}}^{(0)}$ is sometimes denoted χ_{11}, and a high-temperature series expansion was derived up to tenth order in Ref. [32] and up to 23th order in Ref. [33]. As the expressions for anisotropic couplings $K_{\parallel}$ and $K_{\perp}$ become way too complicated, we only give the results for the isotropic Ising model with $K_{\parallel}=K_{\perp}=K$ here: using the definitions $z=\tanh K$, $y=\tanh h_{\mathrm{b}}$ we find

$$m_{\mathrm{b,eq}}(z,y) = \frac{z^{-1}-z}{\frac{z}{y}-\frac{y}{z}}\left[\frac{b^2}{2\pi}\mathrm{K}(16w^2) + \frac{b^2}{4\pi w}\frac{\left(a+\frac{y^2}{z}\right)^2}{1-\frac{by^2}{c^2 z}} \times \Pi\left(\frac{\left(1-\frac{by^2}{z}\right)^2}{1-\frac{by^2}{c^2 z}}, 16w^2\right) + \frac{Y^{1/2}-Y^{-1/2}}{2(z^{-1}-z)} - \frac{1}{4}\right], \tag{A2}$$

$$\chi_{\mathrm{b,eq}}^{(0)}(z) = \left(\frac{1}{z^2}-1\right) \times \left[(1+2w-8w^2)\frac{\mathrm{K}(16w^2)}{4\pi w} - \frac{\mathrm{E}(16w^2)}{4\pi w} - \frac{1}{4}\right], \tag{A3}$$

with the abbreviations

$$w = \frac{z(1-z^2)}{(1+z^2)^2}, \tag{A4a}$$

$$a = \frac{1-2z-z^2}{1+z^2}, \tag{A4b}$$

$$b = \frac{1+2z-z^2}{1+z^2}, \tag{A4c}$$

$$c = \frac{2z}{1+z^2}, \tag{A4d}$$

$$Y = \left(\frac{az}{c^2y^2}+1\right)\left(\frac{by^2}{c^2 z}-1\right)^{-1}, \tag{A4e}$$

and the complete elliptic integrals [37] of the first, second, and third kind, $\mathrm{K}(m)$, $\mathrm{E}(m)$, and $\Pi(n,m)$. Note that the variable w is also used in high-temperature series analysis of the bulk zero-field susceptibility [21]. For $h_{\mathrm{b}}=0$ the surface magnetization Eq. (A2) reduces to the well-known expression

$$m_{\mathrm{b,eq}}(K) = \sqrt{\frac{\cosh 2K - \coth 2K}{\cosh 2K - 1}}. \tag{A5}$$

[1] C. Fusco, D. E. Wolf, and U. Nowak, Phys. Rev. B **77**, 174426 (2008).
[2] M. P. Magiera, L. Brendel, D. E. Wolf, and U. Nowak, EPL **87**, 26002 (2009).
[3] M. P. Magiera, D. E. Wolf, L. Brendel, and U. Nowak, IEEE Trans. Magn. **45**, 3938 (2009).
[4] D. Kadau, A. Hucht, and D. E. Wolf, Phys. Rev. Lett. **101**, 137205 (2008).
[5] C. K. Chan and L. Lin, Europhys. Lett. **11**, 13 (1990).
[6] F. Corberi, G. Gonnella, and A. Lamura, Phys. Rev. Lett. **81**, 3852 (1998).
[7] E. N. M. Cirillo, G. Gonnella, and G. P. Saracco, Phys. Rev. E **72**, 026139 (2005).
[8] T. Imaeda and K. Kawasaki, Prog. Theor. Phys. **73**, 559 (1985).
[9] A. Onuki, J. Phys.: Condens. Matter **9**, 6119 (1997).
[10] S. Katz, J. L. Lebowitz, and H. Spohn, Phys. Rev. B **28**, 1655 (1983).
[11] B. Schmittmann and R. K. P. Zia, in *Phase Transitions and Critical Phenomena*, edited by C. Domb and J. L. Lebowitz (Academic Press, London, 1995), Vol. 17.
[12] M. B. Stearns, in *Magnetic Properties of Metals*, Landolt-Börnstein, New Series, Vol. III/19a, edited by H. P. J. Wijn (Springer, Berlin, 1986).
[13] M. P. Allen and D. J. Tildesley, *Computer Simulation of Liquids* (Clarendon Press, Oxford, 1987).
[14] L. Onsager, Phys. Rev. **65**, 117 (1944).
[15] R. J. Baxter, *Exactly Solved Models in Statistical Mechanics* (Academic Press, London, 1982).
[16] B. M. McCoy and T. T. Wu, *The Two-Dimensional Ising Model*

(Harvard University Press, Cambridge, 1973).
[17] A. M. Ferrenberg and D. P. Landau, Phys. Rev. B **44**, 5081 (1991).
[18] N. Ito, K. Hukushima, K. Ogawa, and Y. Ozeki, J. Phys. Soc. Jpn. **69**, 1931 (2000).
[19] A. Hucht, J. Phys. A **35**, L481 (2002).
[20] S. Angst, A. Hucht, and D. E. Wolf (unpublished).
[21] S. Boukraa, A. J. Guttmann, S. Hassani, I. Jensen, J.-M. Maillard, B. Nickel, and N. Zenine, J. Phys A: Math. Theor. **41**, 455202 (2008), URL http://www.ms.unimelb.edu.au/~iwan/ising/Ising_ser.html
[22] K. Binder and P. C. Hohenberg, Phys. Rev. B **9**, 2194 (1974).
[23] H. Arisue and T. Fujiwara, Nucl. Phys. B (Proc. Suppl.) **119**, 855 (2003); http://www.rccp.tsukuba.ac.jp/kenkyukai/asia-pacific/program/transparency/arisue/asia-pacific2003b@.ps.
[24] R. J. Glauber, J. Math. Phys. **4**, 294 (1963).
[25] K. Kawasaki, Phys. Rev. **145**, 224 (1966).
[26] N. Metropolis, A. W. Rosenbluth, M. N. Rosenbluth, A. H. Teller, and E. Teller, J. Chem. Phys. **21**, 1087 (1953).
[27] W. Kwak, D. P. Landau, and B. Schmittmann, Phys. Rev. E **69**, 066134 (2004).
[28] D. Grüneberg and A. Hucht, Phys. Rev. E **69**, 036104 (2004).
[29] G. Gonnella and M. Pellicoro, J. Phys. A **33**, 7043 (2000).
[30] H. van Beijeren and L. S. Schulman, Phys. Rev. Lett. **53**, 806 (1984).
[31] B. M. McCoy (private communication).
[32] K. Binder and P. C. Hohenberg, Phys. Rev. B **6**, 3461 (1972).
[33] I. G. Enting and A. J. Guttmann, J. Phys. A **13**, 1043 (1980).
[34] M. E. J. Newman and G. T. Barkema, *Monte Carlo Methods in Statistical Mechanics* (Clarendon Press, Oxford, 1999).
[35] TM calculations for stripes of width $L_\perp > 1$ show that this is only the case for $L_\perp = 1$.
[36] Note that Eq. (69) is mentioned in the literature [30,34] without stressing the multiplicative property [Eq. (68)].
[37] We use the definition of elliptic functions without square, e.g., $\mathrm{K}(m) = \int_0^{\pi/2} (1 - m \sin^2 \theta)^{-1/2} \mathrm{d}\theta$.